
ELSEVIER

Computer Physics Communications 102 (1997) 132–146

Computer Physics Communications

Interpolated Differential Operator (IDO) scheme for solving partial differential equations

Takayuki Aoki [1]

Department of Energy Sciences, Tokyo Institute of Technology, 4259 Nagatsuta, Midori-ku, Yokohama 226, Japan

Received 14 October 1996

Abstract

We present a numerical scheme applicable to a wide variety of partial differential equations (PDEs) in space and time. The scheme is based on a high accurate interpolation of the profile for the independent variables over a local area and repetitive differential operations regarding PDEs as differential operators. We demonstrate that the scheme is uniformly applicable to hyperbolic, ellipsoidal and parabolic equations. The equations are solved in terms of the primitive independent variables, so that the scheme has flexibility for various types of equations including source terms. We find out that the conservation holds accurate when a Hermite interpolation is used. For compressible fluid problems, the shock interface is found to be sharply described by adding an artificial viscosity term.

Keywords: Partial differential equation; Hermite interpolation; IDO; Nonconservative form; Numerical scheme
PACS: 02.60.Cd; 02.60.Ed; 02.70.Rw

1. Introduction

Most problems in science and engineering are modeled by partial differential equations (PDEs) in space and time. The motivation to start this study was to construct an accurate approximation for a local domain area by using the governing PDEs as efficiently as possible. Namely, we are able to make use of the equations derived by subsequently differentiating the original equations. Since the domains are connected to each other, we have a discretization scheme for initial boundary problems. Due to the high accurate local interpolated profiles, we expect that high-order schemes for any kind of PDEs will be possible by universal treatment. We construct a high accurate interpolation on the discrete space to an approximate solution profile. The scheme presented in this paper consists of a spatial interpolation and multiple differential operations, and we call this scheme IDO (Interpolated Differential Operator).

For hyperbolic equations, many sophisticated schemes have been presented, for example TVD [1–3], ENO [4–6], PPM [8,9] and others, where successfully good results for compressible fluid problems have been obtained. These schemes solve the hyperbolic equations in a conservative form using a flux correction. In

[1] E-mail: taoki@es.titech.ac.jp

PII S0010-4655(97)00020-9

this paper, we do not transform any independent variable into one taking account of the conservation or characteristics of the given equation. It is necessary to know only the flow direction. The given equations are solved for the primitive variables, so that for hyperbolic equations the scheme becomes nonconservative. Although the scheme loses conservation, it allows a more flexible application to a variety of PDEs, i.e., multicomponent flows [10] and including source terms. Recently, the CIP (Cubic Interpolated Propagation) scheme [11,12] has been presented and applied to many problems [13–15]. In the CIP scheme, the spatial profile is described by a third-order Hermite interpolation in the advection phase and updated by shifting the profile according to the local analytic solution. The CIP scheme for nonconservative form has been developed [16,17], and obtains comparable results with the best of conservative schemes.

A similar scheme DA-CIP has been presented by Utsumi [18]. His scheme applies a third-order Hermite interpolation to the spatial derivative of the given equation. The time integration is split into two stages; fourth-order Runge–Kutta integration and CIP advection. It is shown that the hyperbolic equations are solved successfully. The Kond-P scheme [19] uses Hermite interpolation to solve the diffusion equation. In this paper, the IDO scheme also takes advantage of a Hermite interpolation, however, different interpolations may be used when they describe the higher derivatives with enough accuracy. A rational function [20] or hyper functions are possible candidates.

This paper is organized as follows. In the next section, the basic concept of the IDO scheme is described in detail, and time-integration is described for initial value problems. In Section 3, the relation between CIP and IDO is discussed. Section 4 shows the accuracy of the IDO scheme by solving the mass continuity equation and the Poisson equation. In Section 5, we apply the IDO to various equations and the computational results are presented. In the final section, we give the conclusion and the subjects for further study.

2. Basic concept

In this paper, we present a numerical scheme (Interpolated Differential Operator) IDO for solving hyperbolic, ellipsoidal and parabolic differential equations. The IDO scheme is constructed on the basis of a discrete space (grid points) such as FDM, FEM, and so on. The independent variables defined on the grid have a spatial profile spreading over the local area which covers several grid points. The profile should approximate the solution of the governing PDE within the area. The IDO scheme requires a spatial interpolation describing high-order spatial derivatives accurately.

The given equations are solved in the original differential form described by the primitive independent variables. We regard the derivatives appearing in the equation as differential operators, and we can use the equations derived by temporal and spatial differentiation. We consider the following equation:

$$f_t = \Im_x f\,, \tag{1}$$

where the subscripts t and x denote time and spatial derivative operation, respectively. The symbol $\Im_x$ stands for a spatial differential operator. By taking time derivatives of Eq. (1), we have a series of the equations $f_{tt} = \Im_x \Im_x f$, $f_{ttt} = \Im_x \Im_x \Im_x f, \ldots$, and so on. Higher-order time derivatives are expressed in similar way by successive operations of $\Im_x$. In the IDO scheme, we do not use a finite difference expression for the term, but operate the interpolation profile $F(x)$.

Most schemes for hyperbolic equations use the conservative form, however, the IDO solves it in the primitive form without any transformation of the independent variables. The nonconservative form is more flexibly applicable to various kinds of differential equations with source terms.

2.1. Interpolation

In the IDO scheme, the spatial profiles of the independent variables are spatial interpolation covering several grid points. It is possible to use various interpolations which can describe accurately the spatial derivatives, and in this paper we use a Hermite interpolation which is determined by matching conditions of both the values and the derivatives. The Hermite interpolation has enough accuracy, it requires less computation and the local interpolation area uses only neighboring grid information. We use two kinds of interpolation whose interpolated domain area are different.

Now we consider the interpolation function around the ith grid point in the one-dimensional case. The independent variables f and f_x are assumed to be given at all the grid points. In general, numerical information propagates in all the directions, so that the interpolation has to cover the area from $i-1$ to $i+1$. The Hermite interpolation is obtained by the four matching conditions of $F(-\Delta x) = f_{i-1}$, $F_x(-\Delta x) = f_{x,i-1}$, $F(\Delta x) = f_{i+1}$, and $F_x(\Delta x) = f_{x,i+1}$. The coefficients of the fifth-order polynomial are determined as follows:

$$F(x) = a_c x^5 + b_c x^4 + c_c x^3 + d_c x^2 + f_{x,i} x + f_i \,, \tag{2a}$$

$$a_c = -\frac{3}{4\Delta x^5}(f_{i+1} - f_{i-1}) + \frac{1}{4\Delta x^4}(f_{x,i+1} + 4f_{x,i} + f_{x,i-1}) \,, \tag{2b}$$

$$b_c = -\frac{1}{2\Delta x^4}(f_{i+1} - 2f_i + f_{i-1}) + \frac{1}{4\Delta x^3}(f_{x,i+1} - f_{x,i-1}) \,, \tag{2c}$$

$$c_c = \frac{5}{4\Delta x^3}(f_{i+1} - f_{i-1}) - \frac{1}{4\Delta x^2}(f_{x,i+1} + 8f_{x,i} + f_{x,i-1}) \,, \tag{2d}$$

$$d_c = \frac{1}{\Delta x^2}(f_{i+1} - 2f_i + f_{i-1}) - \frac{1}{4\Delta x}(f_{x,i+1} - f_{x,i-1}) \,. \tag{2e}$$

The derivatives higher than f_x are obtained by differentiating the interpolation function with respect to x. At the ith grid point, we have $f_{xx} = F_{xx}(0) = 2d_c$, $f_{xxx} = F_{xxx}(0) = 6c_c$, $f_{xxxx} = F_{xxxx}(0) = 24b_c$, and $f_{xxxxx} = 120a_c$, and higher derivatives are zero.

Another interpolation is used for the advection term uf_x; for example, $f_t + uf_x = 0$. We call this upwind interpolation. When the advection velocity u is positive, the interpolation covers the area from the $i-1$th to ith grid point. The interpolation function has the following third-order polynomial:

$$F(x) = a_u x^3 + b_u x^2 + f_{x,i} x + f_i \,, \tag{3a}$$

where the coefficients a_u and b_u are determined by the matching conditions $F(-\Delta x) = f_{i-1}$, $F_x(-\Delta x) = f_{x,i-1}$, so that we have

$$a_u = \frac{(f_{x,i} + f_{x,i-1})}{\Delta x^2} - 2\frac{(f_i - f_{i-1})}{\Delta x^3} \,, \quad b_u = \frac{(2f_{x,i} + f_{x,i-1})}{\Delta x} - 3\frac{(f_i - f_{i-1})}{\Delta x^2} \,. \tag{3b}$$

In the case of $u < 0$, the interpolation covers the area from the ith to $i+1$th grid point, and the coefficients are derived by the conditions $F(\Delta x) = f_{i+1}$, $F_x(\Delta x) = f_{x,i+1}$ as follows:

$$a_u = \frac{(f_{x,i} + f_{x,i+1})}{\Delta x^2} + 2\frac{(f_i - f_{i+1})}{\Delta x^3} \,, \quad b_u = -\frac{(2f_{x,i} + f_{x,i+1})}{\Delta x} - 3\frac{(f_i - f_{i+1})}{\Delta x^2} \,. \tag{3c}$$

The derivatives higher than f_x are obtained by taking the derivative of the interpolation function as $f_{xx} = F_{xx}(0) = 2b_u$ and $f_{xxx} = 6a_u$ at the ith grid point, and higher derivatives more than f_{xxx} are set to zero.

In the IDO scheme, the derivative terms included in partial differential equations are classified into an advection term and nonadvection term, and the above two interpolations are applied, respectively.

2.2. Time advance

In the initial-value problem, time integration of the governing equation is done by Taylor expansion for the independent variable with respect to time t. The explicit scheme for time advance is

$$f^{n+1} = f^n + f_t^n \Delta t + f_{tt}^n \frac{\Delta t^2}{2} + f_{ttt}^n \frac{\Delta t^3}{6} + O(\Delta t^4) , \tag{4}$$

$$f_x^{n+1} = f_x^n + f_{tx}^n \Delta t + f_{ttx}^n \frac{\Delta t^2}{2} + f_{tttx}^n \frac{\Delta t^3}{6} + O(\Delta t^4) , \tag{5}$$

where the superscripts $n+1$ and n mean the values in the time $t + \Delta t$ and t, respectively. The series of time derivative of f^n and f_x^n are replaced with the spatial derivative terms by using the original equation. We have a choice to select the order of the Taylor expansion, however, the highest spatial derivative is not able to exceed the order of the interpolated polynomial function. Moreover, there is the upper limit of the time interval Δt due to the numerical stability. We will discuss it in a later paper. At present, we find a proper value of Δt by numerical experiments.

Similarly to Eqs. (4) and (5), the Taylor expansion at $t + \Delta t$ results in an implicit formulation of time advance,

$$f^{n+1} = f^n + f_t^{n+1} \Delta t - f_{tt}^{n+1} \frac{\Delta t^2}{2} + f_{ttt}^{n+1} \frac{\Delta t^3}{6} + O(\Delta t^4) , \tag{6}$$

$$f_x^{n+1} = f_x^n + f_{tx}^{n+1} \Delta t - f_{ttx}^{n+1} \frac{\Delta t^2}{2} + f_{tttx}^{n+1} \frac{\Delta t^3}{6} + O(\Delta t^4) . \tag{7}$$

The numerical technique for solving Eqs. (6) and (7) depends on the governing equation, as it is well known in the techniques of finite difference scheme.

3. Relation to the CIP scheme

Let consider the linear scalar equation $f_t = -u f_x$ with a constant advection velocity (u = const.) as one of the simplest equations. The time derivatives f_t^n, f_{tt}^n and f_{ttt}^n for Eq. (4), and f_{tx}^n, f_{ttx}^n and f_{tttx}^n for Eq. (5) are necessary in order to update f^n and f_x^n at the grid point. Taking the time derivative and substituting $f_t = -u f_x$, we easily derive the series of the following equations:

$$f_{tt} = u^2 f_{xx} , \quad f_{ttt} = -u^3 f_{xxx} , \quad f_{tx} = -u f_{xx} , \quad f_{ttx} = u^2 f_{xxx} , \tag{8}$$

and so on. All the time derivatives are replaced by the spatial derivatives. Applying the upwind interpolation, i.e. Eq. (3a), to this problem, the available highest derivative term is f_{xxx}^n, because the interpolation function is a third-order polynomial. The time accuracy of the Taylor expansion becomes Δt^3 order. Substituting Eqs. (8) into Eqs. (4) and (5), we have

$$\begin{aligned} f^{n+1} &= f^n - u\Delta t f_x^n + \frac{(u\Delta t)^2}{2} f_{xx}^n - \frac{(u\Delta t)^3}{6} f_{xxx}^n \\ &= f^n - u\Delta t f_x^n + (u\Delta t)^2 b_u - (u\Delta t)^3 a_u \\ &= F(-u\Delta t) , \\ f_x^{n+1} &= f_x^n - u\Delta t f_{xx}^n + \frac{(u\Delta t)^2}{2} f_{xxx}^n \\ &= f_x^n - 2u\Delta t b_u + 3(u\Delta t)^2 a_u \end{aligned} \tag{9}$$

$$= F_x(-u\Delta t)\,. \tag{10}$$

It is found that the above two expressions are exactly the same as the procedure of the advection phase of the CIP scheme [16,17], which makes use of the local analytic solution of the advection equation, i.e. $f(t+\Delta t,x) = f(t,x-u\Delta x)$ and $f_x(t+\Delta t,x) = f_x(t,x-u\Delta t)$ at $x=0$. When we substitute Eq. (8) into Eqs. (6) and (7), the implicit expression of the CIP scheme [21] is obtained. It concludes that the IDO scheme involves the CIP advection as a particular case.

4. Accuracy of the IDO scheme

4.1. Mass conservation

Since the IDO scheme is a nonconservative form for the hyperbolic equation, it is useful to check the accuracy of the conservation. We solve the following mass continuity equation:

$$\rho_t + (\rho u)_x = 0\,, \tag{11}$$

$$\rho_{tx} + (\rho u)_{xx} = 0\,, \tag{12}$$

with a steady and nonuniform velocity profile of $u = 1 + a\sin(k_x x)$, where $a = 0.25$. The higher derivatives are derived as follows:

$$\rho_{tt} = -u\rho_{tx} - u_x\rho_t = u^2\rho_{xx} + 3uu_x\rho_x + (u_x^2 + uu_{xx})\rho\,, \tag{13}$$

$$\rho_{ttx} = -u\rho_{txx} - 2u_x\rho_{tx} - u_{xx}\rho_t = u^2\rho_{xxx} + 5uu_x\rho_{xx} + 4(u_x^2 + uu_{xx})\rho_x + (3u_xu_{xx} + uu_{xxx})\rho\,, \tag{14}$$

$$\rho_{ttt} = -u\rho_{ttx} - u_x\rho_{tt}\,, \tag{15}$$

$$\rho_{tttx} = -u\rho_{ttxx} - 2u_x\rho_{ttx} - u_{xx}\rho_{tt}\,, \tag{16}$$

where $\rho_{txx} = -(u\rho)_{xxx}$ and $\rho_{ttxx} = -(u\rho_t)_{xxx}$ are used in Eqs. (14) and (16). We use the upwind interpolation for ρ_{xx} and ρ_{xxx}, and the analytic expression for the derivatives of the velocity. Time integration of Δt^3 order is done by substituting Eqs. (11)–(16) into Eq. (8) with $\Delta t = 0.4$. The results of a total mass conservation $\int \rho\,dx$ is shown in Fig. 1 as a function of the wave number k_x of the velocity profile. The initial density has a square profile; $\rho_i = 1$ for $7 \le i \le 27$ and $\rho_i = 0$ elsewhere. The total mass is integrated at the time $t = 200$ and the mesh interval is $\Delta x = 1$. When we set $\rho_x = 0$ for all the region as an initial condition, the mass conservation error jumps to 10^{-3} at the first time step, and it remains of the same order for greater time. However, by setting initially $\rho_{x,6} = \rho_{x,7} = 0.5$ and $\rho_{x,27} = \rho_{x,28} = -0.5$, we have the remarkably improved result. Fig. 1 shows the deviation rate of the IDO scheme from the initial mass, compared with the result of the finite difference method (FDM) using a nonconservative form of third-order upwind scheme. We use the following finite difference expression for a third-order upwind scheme:

$$\rho_i^{n+1} = \rho_i^n - (u\bar{\rho}_x + \bar{u}_x\rho_i^n)\Delta t + \tfrac{1}{2}(u^2\bar{\rho}_{xx} + 3u\bar{u}_x\bar{\rho}_x + \bar{u}_{xx}\rho_i^n + \bar{u}_x^2\rho_i^n)\Delta t^2\,,$$

where

$$\bar{\rho}_x = (2\rho_{i+1}^n + 3\rho_i^n - 6\rho_{i-1}^n + \rho_{i-2}^n)/6\Delta x\,,$$

$$\bar{\rho}_{xx} = (-\rho_{i+2}^n + 16\rho_{i+1}^n - 30\rho_i^n + 16\rho_{i-1}^n - \rho_{i-2}^n)/12\Delta x^2\,,$$

$$\bar{u}_x = (-u_{i+2} + 8u_{i+1} - 8u_{i-1} + u_{i-2})/12\Delta x^2\,,$$

$$\bar{u}_{xx} = (-u_{i+2} + 16u_{i+1} - 30u_i + 16u_{i-1} - u_{i-2})/12\Delta x^2\,.$$

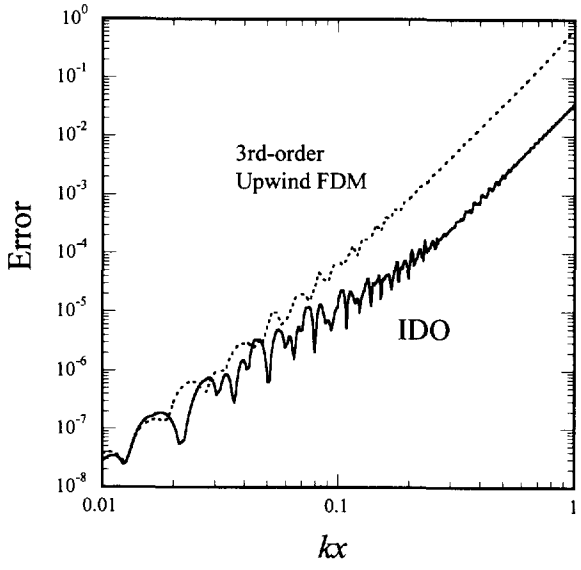

Fig. 1. Mass conservation as a function of velocity nonuniformity k_x, where the velocity profile is $u = 1 + 0.25\sin(k_x x)$. The solid line indicates the result of the IDO after 500 steps with $\Delta t = 0.4$ and $\Delta x = 1$. The dashed line shows the result of third-order upwind FDM of nonconservative form.

It is found that the IDO scheme preserves good accuracy in spite of the nonconservative form even for a large nonuniformity of the advection velocity. The result of the CIP scheme remains in between IDO and FDM.

5. Spatial accuracy

The spatial accuracy of the derivatives obtained by the interpolation can be estimated from the expressions (2a) and (3a), however, the accuracy of the numerical result obtained by the scheme using the derivative formula is not clear. Although there are many publications [16,17] of CIP using upwind Hermite interpolation, the scheme with use of the center Hermite interpolation has not been discussed enough [19]. In order to know the spatial accuracy of the numerical solution, we solve the Poisson equation by the IDO scheme.

For the independent variable f, we solve the original Poisson equation $f_{xx} = \phi$ using the center interpolation, where ϕ is the source term. For another independent variable f_x, we use the additional equation $f_{xxx} = \phi_x$ derived by taking the derivative for the original equation. The explicit descriptions of the discrete formula are written down as follows:

$$\frac{2}{\Delta x^2}(f_{i+1} - 2f_i + f_{i-1}) - \frac{1}{2\Delta x}(f_{x,i+1} - f_{x,i-1}) = \phi_i\,, \tag{17}$$

$$\frac{15}{2\Delta x^3}(f_{i+1} - f_{i-1}) - \frac{3}{2\Delta x^2}(f_{x,i+1} + 8f_{x,i} + f_{x,i-1}) = \phi_{x,i}\,. \tag{18}$$

In the case of $\phi = \sin(k_x x)$ and $k_x = 4\pi$ for $0 \le x \le 1$, we estimate the error of the numerical result f_i by the formula

$$\sigma^2 = \sum_{i=1}^{N}\left(\frac{\sin(k_x x_i)}{k_x^2} - f_i\right)^2\,,$$

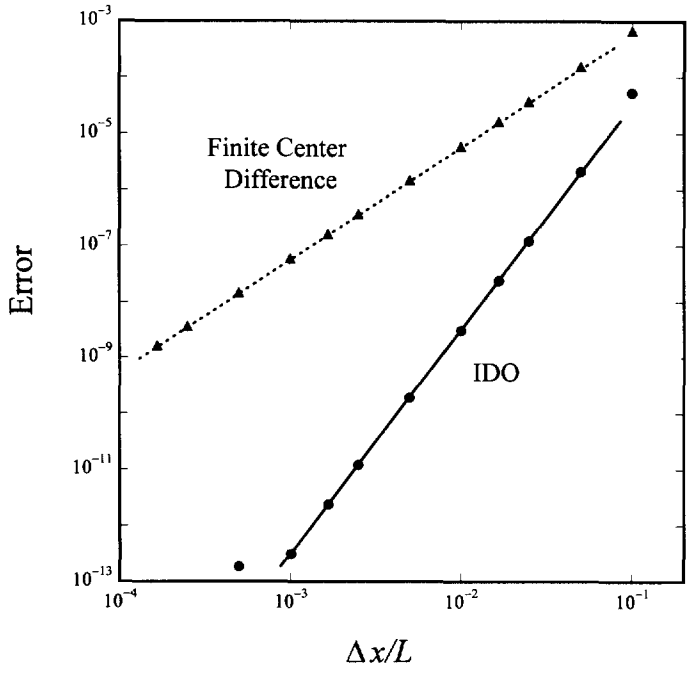

Fig. 2. Spatial accuracy of the numerical solution for the Poisson equation by using the IDO scheme. The solid circles represent the computational result of the IDO scheme showing Δx^4 accuracy, and the solid triangles show Δx^2 accuracy for the result of the center finite difference method $(f_{i+1} - 2f_i + f_{i-1})/\Delta x^2 = \phi_i$.

where N is the total grid number and $\Delta x = 1/(N-1)$. The boundary conditions at $x = 0$ $(i = 1)$ and $x = 1$ $(i = N)$ are $f_1 = f_N = 0$ and $f_{x,1} = f_{x,N} = k_x^{-1}$, respectively. The circles in Fig. 2 show the average error σ of the IDO scheme with the center interpolation as a function of the mesh interval Δx, and it is found that the error has a convergence of Δx^4. As a reference, the results of the finite difference scheme $(f_{i+1} - 2f_i + f_{i-1})/\Delta x^2 = \phi_i$ are plotted by triangular dots, and it has Δx^2 convergence. It is understood that the IDO scheme has the spatial accuracy of Δx^4, since f_{xx} derived from the center interpolation uses five values of the grid and does not use $f_{x,i}$ (see Eq. (17)). In the expression of f_{xxx}, f_i is not included.

6. Numerical experiments

6.1. Nonlinear scalar equation

As examples of nonlinear scalar equations, we examine the shock propagation for the Burgers equation and the traveling soliton waves described by the Korteweg–de Vries (KdV) equation [22]. Both the equations have the same form $u_t + uu_x - f(u) = 0$. Burgers equation takes $f(u) = \kappa u_{xx}$, where κ is a diffusion coefficient. Similarly as in the previous section, we obtain the higher-order time derivatives by differentiating the governing equation as follows:

$$u_t = -uu_x + \kappa \tilde{u}_{xx}\,, \tag{19a}$$

$$u_{tx} = -uu_{xx} - u_x^2 + \kappa \tilde{u}_{xxx}\,, \tag{19b}$$

$$u_{tt} = -u_t u_x - uu_{tx} + \kappa u_{txx}\,, \tag{19c}$$

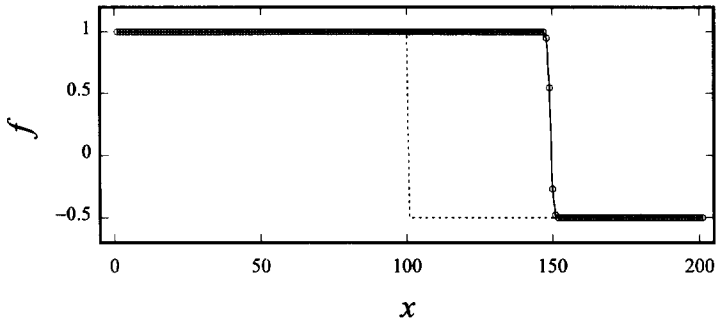

Fig. 3. The profiles of the numerical solution of the Burgers equation at $t = 200$. The initial profile is indicated by the dashed line. The speed of the shock front is found to be 0.25.

$$u_{ttx} = -u_{tx}u_x - u_t u_{xx} - u_x u_{tx} - u u_{txx} + \kappa u_{txxx} . \tag{19d}$$

Here, by using $u_{txx} = -uu_{xxx} - 3u_x u_{xx} + \kappa \tilde{u}_{xxxx}$ and $u_{txxx} = -uu_{xxxx} - 4u_x u_{xxx} - 3u_{xx}^2 + \kappa \tilde{u}_{xxxxx}$, the left-hand side terms of Eq. (19b) and (19c) are replaced by spatial derivative terms. We substitute the above equations into the explicit Taylor expansion to perform a time evolution. We apply the upwind interpolation to the derivative terms derived from the advection term, and the center interpolation to the diffusion term; the derivative terms with the symbol ˜ use the center interpolation, while the other terms are from the upwind interpolation. In this section, we truncate the Taylor expansion up to Δt^2. In order to describe the shock discontinuity, we have added the diffusion term with a small diffusion coefficient, because the IDO scheme is a nonconservative form. The initial condition is the following: $u = a$ for $x < 50$ and $u = b$ for $x \geq 50$ at the time $t = 0$. According to the weak solution of the conservation law, the shock speed is equal to $(a + b)/2$. The grid spacing is $\Delta x = 1$. When we set $a = 1$, $b = -0.5$ and $\kappa = 0.3$, the computational result at the time $t = 200$ is plotted by the dots in Fig. 3. The dashed line indicates the initial state. The shock speed appears to be 0.25 and it is in a good agreement with the weak solution. In the case of a larger κ (for example $\kappa = 1$), the profile of the shock interface becomes more diffusive, however, the shock speed is the same as that of $\kappa = 0.3$.

In the case of a KdV equation, we replace the κu_{xx} term with $-\delta^2 u_{xxx}$ and neglect the derivatives higher than u_{xxx} for the upwind interpolation, and higher than $\tilde{u}_{xxxxx}$ for the center interpolation. The procedure is similar as with the Burgers equation, and a modified point is to use $\tilde{\tilde{u}}_{xxx} = (u_{x,i+1} - 2u_{x,i} + u_{x,i-1})/\Delta x^2$ for the dispersion term instead of the center interpolation equation (2d). Namely, we use the following equation:

$$u_t = -uu_x - \delta^2 \tilde{\tilde{u}}_{xxx} \tag{20}$$

in order to keep the stability and conservation for a particular case. To check the scheme, we compute the traveling soliton waves. The initial condition is the same as in Ref. [23], and it is shown in Fig. 4 by the dotted line; $u_i = \cos kx_i$, $u_{x,i} = -k \sin kx_i$, $k = \pi$, $\Delta x = 2.0/N$, $x_i = (i - 1)\Delta x$, $N = 192$. The numerical result at $t = 1.6/\pi$ is indicated by the dot-dashed line and the result at $t = 3.6/\pi$ is shown by the solid line. It is found that both the results agree well with the results in Ref. [23].

6.2. Wave equation

The wave equation described by $f_{tt} - c^2 f_{xx} = 0$ includes both the right traveling wave and left traveling wave. By factorization, we have $(\partial_t - c\partial_x)(\partial_t + c\partial_x) f = 0$ and split this into $f_t + cf_x = g$ and $g_t - cg_x = 0$, where the symbol c is a positive constant. These two equations are easily solved by many numerical schemes, however, it is impossible to factorize the multi-dimensional wave equation. The IDO scheme is capable to solve the form $f_{tt} - c^2 f_{xx} = 0$ straightforwardly. According to the Taylor expansions (4) and (5), odd-order time

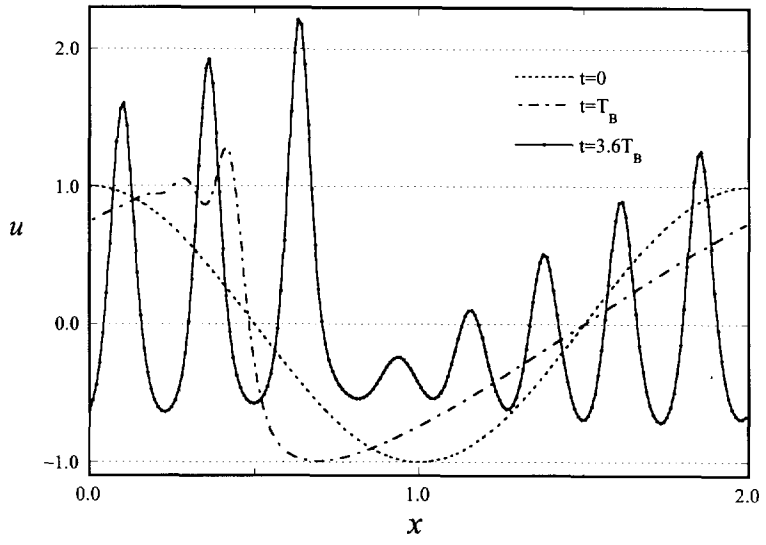

Fig. 4. The numerical results of the KdV equation with $\Delta x = 1/192$. The dashed line is the initial profile. The dot dashed line is the profile of $t = 1/\pi$, and the solid line shows that of $t = 3.6/\pi$.

derivatives are required additionally, so that we use f_t and f_{tx} as new independent variables. Taking the time derivative of Eqs. (4) and (5), we have the following equations:

$$f^{n+1} = f^n + f_t^n \Delta t + c^2 f_{xx}^n \frac{\Delta t^2}{2} + c^2 f_{txx}^n \frac{\Delta t^3}{6} + c^4 f_{xxxx}^n \frac{\Delta t^4}{24} + O(\Delta t^5)\,, \tag{21a}$$

$$f_x^{n+1} = f_x^n + f_{tx}^n \Delta t + c^2 f_{xxx}^n \frac{\Delta t^2}{2} + c^2 f_{txxx}^n \frac{\Delta t^3}{6} + c^4 f_{xxxxx}^n \frac{\Delta t^4}{24} + O(\Delta t^5)\,, \tag{21b}$$

$$f_t^{n+1} = f_t^n + c^2 f_{xx}^n \Delta t + c^2 f_{txx}^n \frac{\Delta t^2}{2} + c^4 f_{xxxx}^n \frac{\Delta t^3}{6} + c^4 f_{txxxx}^n \frac{\Delta t^4}{24} + O(\Delta t^5)\,, \tag{21c}$$

$$f_{tx}^{n+1} = f_{tx}^n + c^2 f_{xxx}^n \Delta t + c^2 f_{txxx}^n \frac{\Delta t^2}{2} + c^4 f_{xxxxx}^n \frac{\Delta t^3}{6} + c^4 f_{txxxxx}^n \frac{\Delta t^4}{24} + O(\Delta t^5)\,. \tag{21d}$$

Deriving Eqs. (21a)–(21d), we use the relations $f_{tt} = c^2 f_{xx}$ and $f_{tttt} = c^4 f_{xxxx}$, and these spatial derivatives. Since we use the center interpolation of the fifth-order polynomial, higher derivatives than f_{xxxxx} are neglected and the time accuracy of this scheme becomes Δt^5. The initial value problem of the wave propagation is examined with the above scheme. Fig. 5 shows the computational result with $c = 1$ at $t = 50$, and the dashed lines indicate the initial profile of f. When we give the initial time derivatives of $f_t = cf_x$ and $f_{tx} = cf_{xx}$, a right traveling wave appears as is shown in Fig. 5a. The initial conditions of $f_t = -cf_x$ and $f_{tx} = -cf_{xx}$ generate a left traveling wave (Fig. 5c). In the case of $f_t = 0$ and $f_{tx} = 0$, the profile is split into two waves traveling with half amplitude in both directions (Fig. 5b). The results are enough for most initial profiles by computing Eq. (21), however, a small numerical oscillation appears for the profile with very steep gradients. To smear the oscillation, we add the viscous term $0.2c^2 f_{txx}\Delta t^2$ in Eq. (21c) and $2c^2 f_{txxx}\Delta t^2$ in Eq. (21d), and obtain a less oscillating result.

6.3. 1D Riemann problem

We study the Riemann initial value problem for the Euler equations as a more complicated hyperbolic equation. The employed equations for density, velocity and internal energy are as follows:

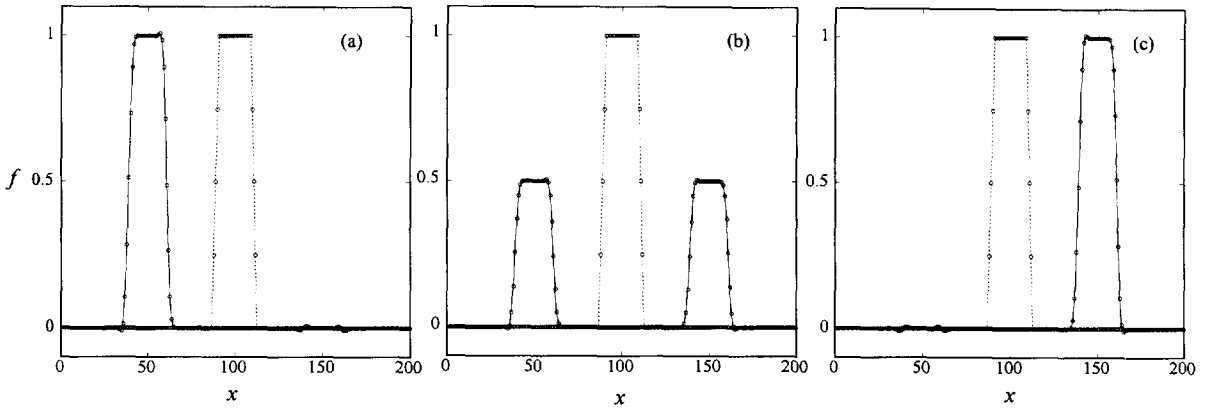

Fig. 5. The results of wave equation by using IDO with the center interpolation. The dashed lines show the initial profile. When the initial conditions of the first time derivative are $f_t = cf_x$ and $f_t = -cf_x$, the results show a left traveling wave (a) and a right traveling wave (c), respectively. When the initial time derivative is zero, the profile is split into two waves (b).

$$\rho_t = -(\rho u)_x\,, \tag{22a}$$

$$u_t = -uu_x - \frac{P_x}{\rho}\,, \tag{22b}$$

$$e_t = -ue_x - \frac{P}{\rho}u_x\,. \tag{22c}$$

Using these equations, we can derive the set of higher time derivatives $\{\rho_t, \rho_{tt}, \rho_{ttt}, \rho_{tx}, \rho_{ttx}, \rho_{tttx}, u_t, u_{tt}, u_{ttt}, u_{tx}, u_{ttx}, u_{tttx}, e_t, e_{tt}, e_{ttt}, e_{tx}, e_{ttx}, e_{tttx}\}$, whose derivations are shown in the appendix. All the independent variables ρ, u, e and their derivatives are defined at the same grid point, and we do not use any staggered grid systems. The initial condition is $\rho = 1$, $P = 1$ for the leftmost 100 zones and $\rho = 0.125$, $P = 0.1$ for the other zones; $u = 0$ and $\gamma = 1.4$ in all zones and $\Delta x = 0.01$. As it is mentioned in Section 4, an artificial viscosity q has to be added to the pressure term in order to describe the shock interface. We use a differential form of the von Neumann–Richtmyer type [24] $q = \alpha\rho c_s u_x$ (c_s is sound speed) only for the compression region, where the minimum of $u_{x,i-1}$, $u_{x,i}$ and $u_{x,i+1}$ is negative and α is a constant of order of unity. The computational profile of the density is given in Fig. 6 by the open circles, and the solid line is the analytic solution. At the contact discontinuity, a small undershoot and overshoot appears as in the case of CIP [16,17] and DA-CIP [18] schemes. The sharpness of the shock interface depends on the value α, and the computation becomes unstable for $\alpha < 0.3$.

6.4. *Two interacting blast waves*

For a complicated compressible fluid motion, we examine two interacting blast waves which were reviewed in details in [5–7,9]. The initial condition consists of three constant states of gamma-law gas with $\gamma = 1.4$; the density is everywhere unity, the pressure is equal to 1000 in the leftmost tenth, and 100 in the rightmost, while in between it is equal to 0.01. Both the boundaries are reflecting wall separated by a distance of unity. Two strong shock waves develop and collide interacting with rarefaction waves reflected at the boundary. We have used the same scheme as in the case of the previous shock problem. The mesh interval used in this calculation is 1/800 uniformly. Figs. 7a and b show the velocity and density profiles at time $t = 0.016$. The density jump has good agreement with the conservation law, however, small overshoots appear at the contact discontinuity sides. In Figs. 7c and d, the profiles at time $t = 0.038$ are shown. The collision of shock waves produces new contact discontinuities and the density profile becomes quite complicated. The small overshoots which appear

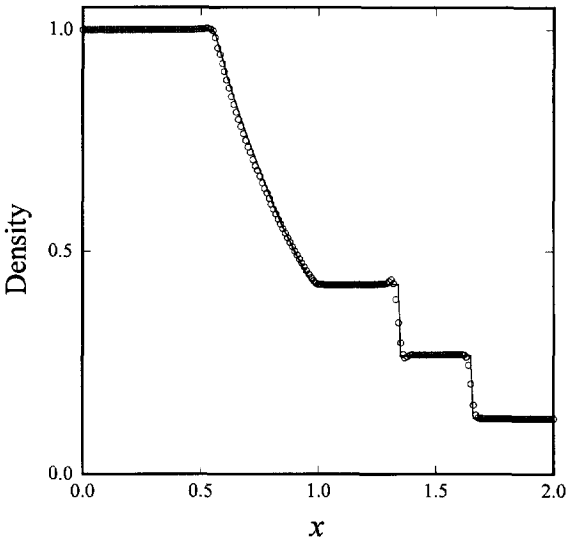

Fig. 6. The results of applying the IDO scheme to the Riemann problem. The initial profile is $\rho = 1$, $u = 0$, $P = 1$ for $x < 1$ and $\rho = 0.125$, $u = 0$, $P = 0.1$ for $x \geq 1$. The solid line shows the analytic solution, and the open circles denote the computational result of the density profile.

in Fig. 7b still exist at this time. The contours of the density in space-time is shown in Fig. 8. Sixty contours are drawn in equally spaced. Although we use only 800 meshes, the results in Figs. 7 and 8 are in excellent agreement with the results of [9] where 3096 mesh points were used.

7. Conclusion

In this paper, we have presented the IDO scheme for solving various kinds of partial differential equations. The independent variables defined at the grid have a spatial profile with the Hermite interpolation which is determined by the values and the first spatial derivatives of the neighboring grids. We use two interpolations which have different interpolation areas, and the upwind interpolation is applied only to the advection term. When we use the center interpolation of the fifth polynomial to solve the Poisson equation, the numerical solution is found to be Δx^4 convergent. We have used the IDO scheme for the mass continuity equation, and the total mass conservation is preserved with a very good accuracy in spite of the nonconservative form. Applications of the IDO scheme to nonlinear scalar equations, a wave equation and Riemann problems have been performed straightforwardly with the same procedure, and good results have been obtained. It is concluded that the IDO scheme is uniformly applicable to hyperbolic, ellipsoidal and parabolic equations and it is easy to construct the numerical discretization scheme with the same procedure.

For all the numerical experiment presented in this paper, we have demonstrated stable computations by a proper chose of Δt. In the next work, we intend to investigate the numerical stability of the IDO scheme. We have discussed a one-dimensional IDO scheme throughout the paper. Because the scheme does not depend on the characteristics of the equations, we expect that the IDO scheme can be extended to the multi-dimensional case without difficulties, which will be also done in the next paper.

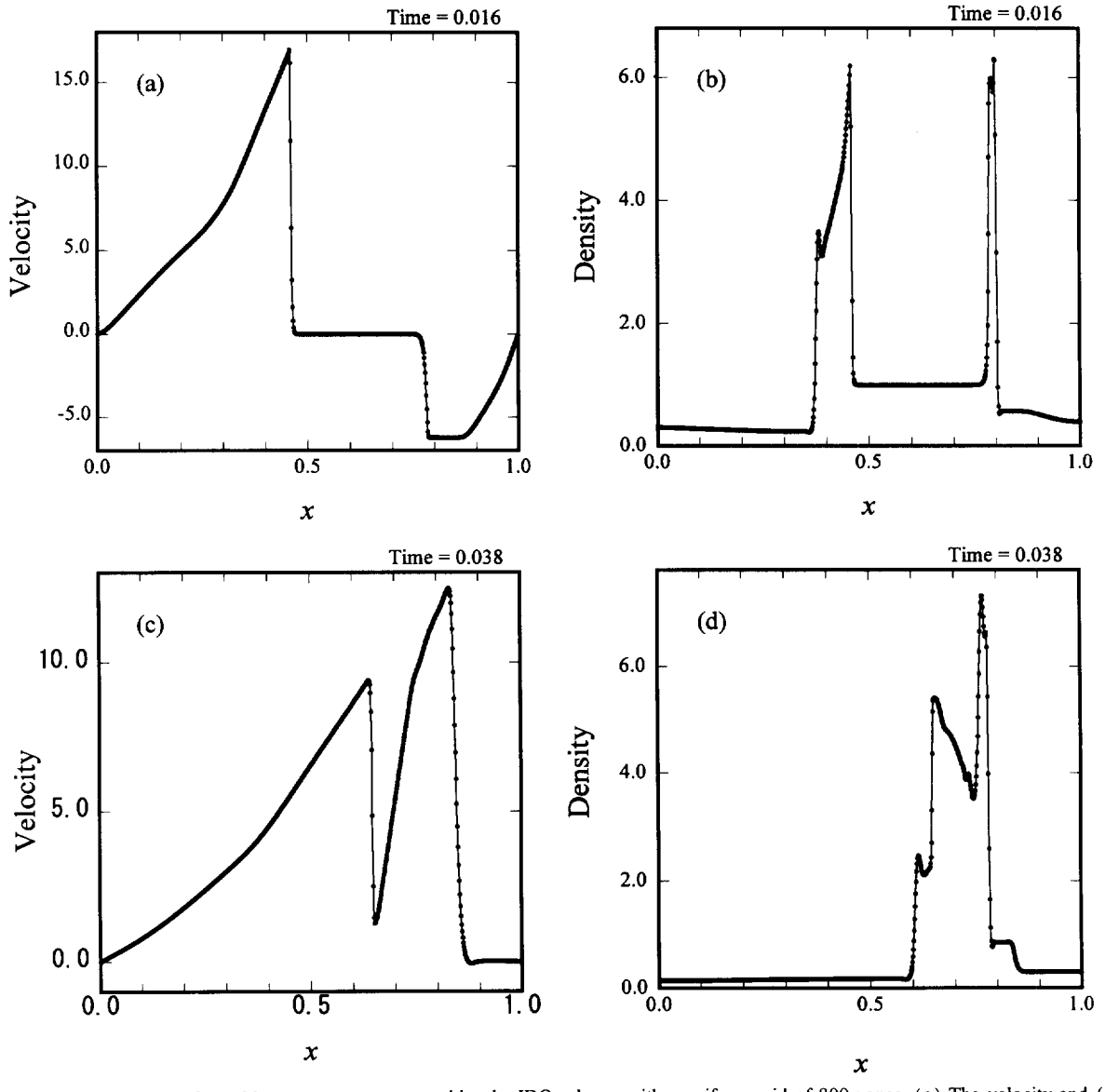

Fig. 7. The interaction of two blast waves are computed by the IDO scheme with a uniform grid of 800 zones. (a) The velocity and (b) density profiles of $t = 0.016$ are shown in the upper half, and those of $t = 0.038$ are shown in the lower half ((c) and (d), respectively).

Acknowledgements

The author would like to thank Prof. Yabe for useful comments and encouragement. This work was supported by Research Foundation for Opto-Science and Technology.

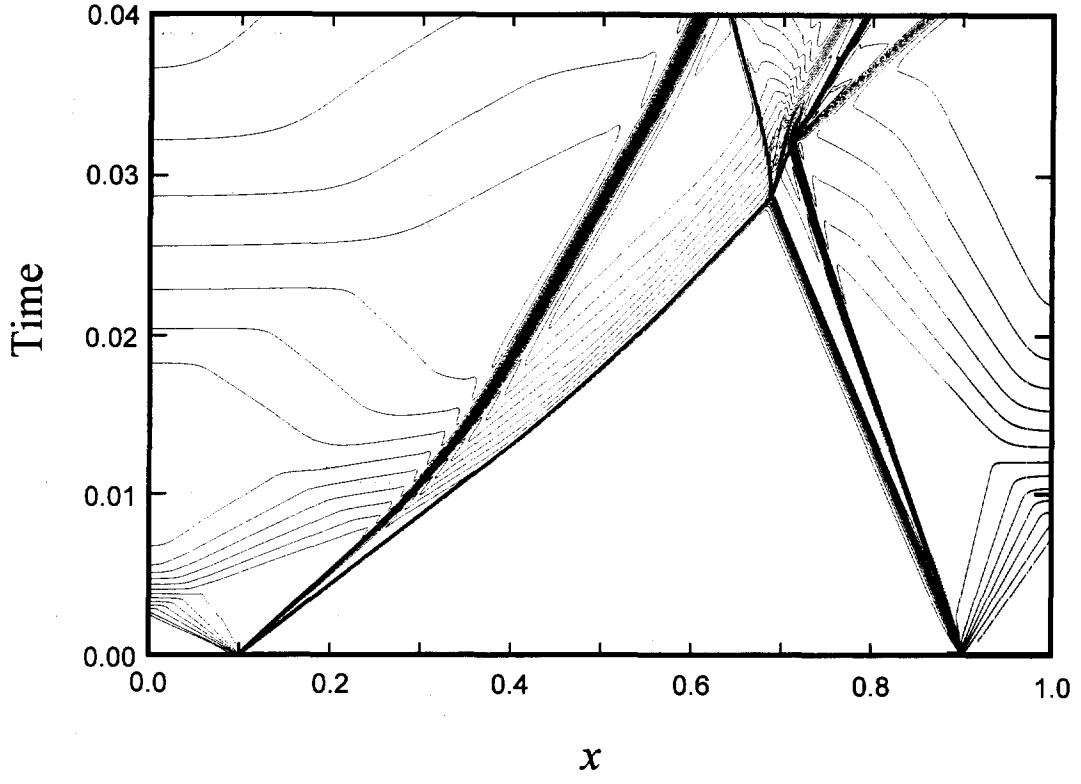

Fig. 8. Contours of density in the space-time plane for the interacting blast wave problem. Sixty contours equally spaced in $\log \rho$ are shown.

Appendix A. IDO formulation for the Euler equation

We derive the IDO scheme for the one-dimensional Euler equations (22a)–(22c) in the explicit form

$$\rho_t = -\rho_x u - \rho u_x , \tag{A.1}$$

$$\rho_{tx} = -\rho_{xx} u - 2\rho_x u_x - \rho u_{xx} , \tag{A.2}$$

$$u_t = -u u_x - (P_x + q_x)/\rho , \tag{A.3}$$

$$u_{tx} = -u_x^2 - u u_{xx} - (P_{xx} + q_{xx})/\rho + (P_x + q_x)\rho_x/\rho^2 , \tag{A.4}$$

$$e_t = -u e_x - (P + q)u_x/\rho , \tag{A.5}$$

$$e_{tx} = -u_x e_x - u e_{xx} - (P_x + q_x)u_x/\rho - (P + q)\tilde{u}_{xx}/\rho + (P + q)u_x\rho_x/\rho^2 , \tag{A.6}$$

$$\rho_{txx} = -\rho_{xxx} u - 3\rho_{xx} u_x - 3\rho_x u_{xx} - \rho u_{xxx} , \tag{A.7}$$

$$\begin{aligned} u_{txx} = {} & -3u_x u_{xx} - u u_{xxx} - (P_{xxx} + q_{xxx})/\rho + 2(P_{xx} + q_{xx})\rho_x/\rho^2 + (P_x + q_x)\rho_{xx}/\rho^2 \\ & - 2(P_x + q_x)\rho_x^2/\rho^3 , \end{aligned} \tag{A.8}$$

$$\begin{aligned} e_{txx} = {} & -u_{xx} e_x - 2u_x e_{xx} - u e_{xxx} - (P_{xx} + q_{xx})u_x/\rho - 2(P_x + q_x)\tilde{u}_{xx}/\rho + 2(P_x + q_x)u_x\rho_x/\rho^2 \\ & - (P + q)\tilde{u}_{xxx}/\rho + 2(P + q)\tilde{u}_{xx}\rho_x/\rho^2 + (P + q)u_x\tilde{\rho}_{xx}/\rho^2 + (P + q)u_x\rho_x^2/\rho^3 . \end{aligned} \tag{A.9}$$

The derivatives ρ_{txx}, u_{txx} and e_{txx} are derived in advance, and are used in order to obtain the following higher time derivatives:

$$\rho_{tt} = -\rho_{tx}u - \rho_x u_t - \rho_t u_x - \rho u_{tx}\,, \tag{A.10}$$

$$\rho_{ttx} = -\rho_{txx}u - \rho_{xx}u_t - 2\rho_{tx}u_x - 2\rho_x u_{tx} - \rho_t u_{xx} - \rho u_{txx}\,, \tag{A.11}$$

$$u_{tt} = -u_t u_x - u u_{tx} - (P_{tx} + q_{tx})/\rho + (P_x + q_x)\rho_t/\rho^2\,, \tag{A.12}$$

$$\begin{aligned} u_{tx} = {} & -2u_{tx}u_x - u_t u_{xx} - u u_{txx} - (P_{txx} + q_{txx})/\rho + (P_{xx} + q_{xx})\rho_t/\rho^2 \\ & + (P_{tx} + q_{tx})\rho_x/\rho^2 + (P_x + q_x)\rho_{tx}/\rho^2 + (P_x + q_x)\rho_x\rho_t/\rho^3\,, \end{aligned} \tag{A.13}$$

$$e_{tt} = -u_t e_x - u e_{tx} - (P_t + q_t)u_x/\rho - (P + q)u_{tx}/\rho + (P + q)u_x\rho_t/\rho^2\,, \tag{A.14}$$

$$\begin{aligned} e_{ttx} = {} & -u_{tx}e_x - u_x e_{tx} - u_t e_{xx} - u e_{txx} - (P_{tx} + q_{tx})u_x/\rho - (P_x + q_x)u_{tx}/\rho \\ & + (P_x + q_x)u_x\rho_t/\rho^2 - (P_t + q_t)\tilde{u}_{xx}/\rho - (P + q)u_{txx}/\rho + (P + q)\tilde{u}_{xx}\rho_t/\rho^2 \\ & + (P_t + q_t)u_x\rho_x/\rho^2 + (P + q)u_{tx}\rho_x/\rho^2 + (P + q)u_x\rho_{tx}/\rho^2 - 2(P + q)u_x\rho_x\rho_t/\rho^3\,. \end{aligned} \tag{A.15}$$

For the ideal equation of state, the pressure P which is a function of ρ and e is written by $P = (\gamma - 1)\rho e$, and the derivatives are derived as follows:

$$P_x = P_\rho\rho_x + P_e e_x = (\gamma - 1)(\rho_x e + \rho e_x)\,, \tag{A.16}$$

$$P_{xx} = (\gamma - 1)(\tilde{\rho}_{xx} + 2\rho_x e_x + \rho\tilde{e}_{xx})\,, \tag{A.17}$$

$$P_{xxx} = (\gamma - 1)(\tilde{\rho}_{xxx}e + 3\tilde{\rho}_{xx}e_x + 3\rho_x\tilde{e}_{xx} + \rho\tilde{e}_{xxx})\,, \tag{A.18}$$

$$P_{tx} = (\gamma - 1)(\rho_{tx}e + \rho_x e_t + \rho_t e_x + \rho e_{tx})\,, \tag{A.19}$$

$$P_{txx} = (\gamma - 1)(\rho_{txx}e + \tilde{\rho}_{xx}e_t + 2\rho_{tx}e_x + 2\rho_x e_{tx} + \rho_t\tilde{e}_{xx} + \rho e_{txx})\,. \tag{A.20}$$

For artificial viscosity, we use the expression $q = \alpha\rho c_s u_x$, and the derivatives are

$$q_x = \alpha c_s(\rho_x u_x + \rho\tilde{u}_{xx})\,, \tag{A.21}$$

$$q_{xx} = \alpha c_s(\tilde{\rho}_{xx}u_x + 2\rho_x\tilde{u}_{xx} + \rho\tilde{u}_{xxx})\,, \tag{A.22}$$

$$q_{xxx} = \alpha c_s(\tilde{\rho}_{xxx}u_x + 3\tilde{\rho}_{xx}\tilde{u}_{xx} + 3\rho_x\tilde{u}_{xxx} + \rho\tilde{u}_{xxxx})\,, \tag{A.23}$$

$$q_{tx} = \alpha c_s(\rho_{tx}u_x + \rho_x u_{tx} + \rho_t\tilde{u}_{xx} + \rho u_{txx})\,, \tag{A.24}$$

$$q_{txx} = \alpha c_s(\rho_{txx}u_x + \tilde{\rho}_{xx}u_{tx} + 2\rho_{tx}\tilde{u}_{xx} + 2\rho_x u_{txx} + \rho_t\tilde{u}_{xxx} + \rho u_{txxx})\,, \tag{A.25}$$

where we neglect the dependency of e on the sound speed c_s.

These derivatives are substituted into the following explicit Taylor expansions to update to the time step $t + \Delta t$:

$$\rho^{n+1} = \rho^n + \rho_t^n\Delta t + \tfrac{1}{2}\rho_{tt}^n\Delta t^2\,, \tag{A.26}$$

$$\rho_x^{n+1} = \rho_x^n + \rho_{tx}^n\Delta t + \tfrac{1}{2}\rho_{ttx}^n\Delta t^2\,, \tag{A.27}$$

$$u^{n+1} = u^n + u_t^n\Delta t + \tfrac{1}{2}u_{tt}^n\Delta t^2\,, \tag{A.28}$$

$$u_x^{n+1} = u_x^n + u_{tx}^n\Delta t + \tfrac{1}{2}u_{ttx}^n\Delta t^2\,, \tag{A.29}$$

$$e^{n+1} = e^n + e_t^n\Delta t + \tfrac{1}{2}e_{tt}^n\Delta t^2\,, \tag{A.30}$$

$$e_x^{n+1} = e_x^n + e_{tx}^n\Delta t + \tfrac{1}{2}e_{ttx}^n\Delta t^2\,. \tag{A.31}$$

The time accuracy of Δt^2 is enough for the CFL number less than 0.2. In the above equations, the derivatives with the symbol tilde ˜ denote the center interpolation for equal to or higher than second derivative; the derivatives without tilde come from the upwind derivative.

References

[1] A. Harten, J. Comput. Phys. 49 (1983) 357.
[2] H. Yang, J. Comput. Phys. 89 (1990) 125.
[3] S. Osher and S. Chakravarthy, SIAM J. Numer. Anal. 21 (1984) 955.
[4] A. Harten, J. Comput. Phys. 71 (1987) 231.
[5] A. Harten, J. Comput. Phys. 83 (1989) 148.
[6] C-W. Shu and S. Osher, J. Comput. Phys. 83 (1989) 32.
[7] H. Nessyahu and E. Tadmor, J. Comput. Phys. 87 (1990) 408.
[8] P. Colella and P.R. Woodward, J. Comput. Phys. 54 (1984) 174.
[9] P. Woodward and P. Colella, J. Comput. Phys. 54 (1984) 115.
[10] S. Karni, J. Comput. Phys. 112 (1994) 31.
[11] H. Takewaki, A. Nishiguchi and T. Yabe, J. Comput. Phys. 61 (1985) 261.
[12] H. Takewaki and T. Yabe, J. Comput. Phys. 70 (1987) 355.
[13] T. Yabe, Rev. Laser Eng. 20 (1992) 691.
[14] T. Yabe and F. Xiao, J. Phys. Soc. Jpn 62 (1993) 2537.
[15] T. Yabe et al., Geophys. Res. Lett. 22 (1995) 2429.
[16] T. Yabe and E. Takei, J. Phys. Soc. Jpn 57 (1988) 2598.
[17] T. Yabe and T. Aoki, Comput. Phys. Commun. 66 (1991) 219.
[18] T. Utsumi, Comput. Fluid Dynamics J. 4 (1995) 225.
[19] Y. Kondoh, Y. Hosaka and K. Ishii, Comput. Math. Appl. 27 (1994) 59.
[20] F. Xiao, T. Yabe, G. Nizam and T. Itoh, Comput. Phys. Commun. 93 (1996) 1.
[21] M. Ida and T. Yabe, Comput. Phys. Commun. 92 (1995) 21.
[22] D.J. Korteweg and de Vries, Philos. Mag. Ser. 5 (1895) 422.
[23] N.J. Zabusky and M.D. Kruskal, Phys. Rev. Lett. 15 (1965) 240.
[24] J. von Neumann and R.D. Richtmyer, J. Appl. Phys. 21 (1950) 232.